

# Structure, defect substructure and fracture surface of low-carbon alloy steel welds

*N. A. Kozyrev, Dr. Eng., Prof., Head of the Dept. of Materials Science, Foundry and Welding Production<sup>1</sup>;*

*R. E. Kryukov, Cand. Eng., Associate Prof., Dept. of Materials Science, Foundry and Welding Production<sup>1</sup>;*

*V. E. Gromov, Dr. Phys.-Math., Prof., Head of the Dept. of Natural Sciences named after prof. V. M. Finkel<sup>1</sup>, e-mail: gromov@physics.sibsiu.ru;*

*Yu. A. Shliarova, Postgraduate Student, Dept. of Natural Sciences named after prof. V. M. Finkel<sup>1</sup>*

<sup>1</sup>*Siberian State Industrial University (Novokuznetsk, Russia)*

By the methods of scanning and transmission electron microscopy a structural phase state, defect substructure and fracture surface of low carbon alloy steel welds produced with use of carbon-containing addition and without it are investigated. The study of etched metallographic section structure of welds revealed a presence of a large amount of second phase particles (carbides, sulfides, oxides, etc.). It is shown that in weld with a carbon-containing addition the particles locate chaotically, and in weld without addition they decorate boundaries of ferrite grains. Dimensions of second phase particles vary in the limits from 0.8  $\mu\text{m}$  to 5  $\mu\text{m}$  and are identical for both types of welds. Analysis of fracture surface structure of welds is carried out. A presence of nonmetallic inclusions is detected. They are typical of mainly weld produced without a carbon-containing addition which may indicate its increased brittleness. Amount of micropores in fracture of weld with carbon-containing addition is many times greater than that in weld without addition, which is indicative of gas removal in use of carbon-containing addition. The quantitative analysis of structure and dislocation substructure parameters of weld metal is carried out, the estimates of contributions of scalar and excess dislocation density to strength of welds are performed. It is shown that higher values of scalar and excess dislocation density in the weld formed without carbon-containing addition in flux may be responsible for material embrittlement. A large quantity of stress concentrators in the weld without carbon-containing addition may result in material embrittlement.

**Key words:** weld seam, fractography, structure, defect substructure, phase composition, fracture surface, dislocations, low carbon steel.

**DOI:** 10.17580/cisr.2022.01.15

## Introduction

The indispensable elements of majority of constructions are welded joints. A structural phase state of metal, being formed in the process of welding and being determined by its regimes and methods, influences the physical-mechanical properties of products. High rates of development of the territories in the Far North accentuated the problem of quality of welding of metal constructions being in service at low temperatures. A fundamental task is to produce welded joint with high operating characteristics providing the increase in reliability of work of fabricated metal products under the extreme conditions [1-5].

Physical-mechanical properties of welded-joints depend not only on weld metal composition but also on content of nonmetallic inclusions in it. The majority of nonmetallic inclusions being detected in welds are oxide compounds of exogenic and endogenic character formed as a result of metal reduction by silicon and manganese. To overcome this disadvantage it is necessary to use carbon-containing fluxes or additives to them [6, 7].

The purpose of the research is to study a structural phase state, dislocation substructure and fracture surface of welds produced with use of carbon-containing addition and without it.

## Material and technique of study

The submerged arc welding based on slag of silicomanganese production with use of carbon containing addition (weld 1) and without it (weld 2) was done in butt manner without bevel from two sides on samples 500 mm  $\times$  75 mm  $\times$  16 mm (thick) in size from sheet steel of 09G2S (09Mn2Si) grade. The sizes of samples and weld type met the requirements for certification of technology and materials for welding. The chemical composition of carbon-containing addition according to Technical Specification TS 5929-007-01395874-2015 (mass. %) is the following:  $\text{Al}_2\text{O}_3$  – 21-46.23; F – 18-27;  $\text{Na}_2\text{O}$  – 8-15;  $\text{K}_2\text{O}$  – 0.4-6.0;  $\text{CaO}$  – 0.7-2.3;  $\text{SiO}_2$  – 0.5-2.48;  $\text{Fe}_2\text{O}_3$  – 2.1-3.27; C – 12.5-30.2;  $\text{MnO}$  – 0.07-0.9;  $\text{MgO}$  – 0.06-0.9; S – 0.1-2.05; P – 0.1-0.18. The material consists of two-dimensional ordered carbon ( $d_{002} = 3.47 \text{ \AA}$ ,  $L_c = 45.8 \text{ \AA}$ ), X-ray amorphous substance, cryolite, corundum, chiolite and different impurities. The process was performed by wire Sv-08GA using a welding plant ASAW-150 and regimes:  $I = 700 \text{ A}$ ;  $U = 30 \text{ V}$ . The elemental composition of weld metal samples under study is listed in the **Table 1**.

The chemical composition of flux from slag of silicomanganese production (mass.%) is the following:

Weld	C	Si	Mn	Cr	Ni	Cu	Nb	Al	S	P
1	0.12	0.66	1.43	0.02	0.06	0.10	0.011	0.012	0.027	0.008
2	0.09	0.71	0.51	0.03	0.10	0.11	0.014	0.023	0.018	0.012

$\text{Al}_2\text{O}_3$  – 6.91-9.62;  $\text{CaO}$  – 22.85-31.70;  $\text{SiO}_2$  – 46.46-48.16;  $\text{FeO}$  – 0.27-0.81;  $\text{MgO}$  – 6.48-7.92;  $\text{MnO}$  – 8.01-8.43;  $\text{F}$  – 0.28-0.76;  $\text{Na}_2\text{O}$  – 0.26-0.36;  $\text{K}_2\text{O}$  – up to 0.62;  $\text{S}$  – 0.15-0.17;  $\text{P}$  – 0.01.

The fracture surface structure and etching surface of weld metal were analyzed by the methods of scanning electron microscopy (SEM). The etching of samples' surface was performed by pulsed electron beam irradiation on setup "SOLO" [8]. The parameters of irradiation were the following: energy of accelerated electrons – 18 keV, energy density of electron beam –  $10 \text{ J/cm}^2$ , duration of electron beam pulse –  $50 \mu\text{s}$ , pulse number – 3, pulse repetition rate –  $0.3 \text{ s}^{-1}$ , irradiation was performed

in the medium of residual inert gas (argon) under pressure of 0.02 Pa. The study of phase morphology, defect substructure and phase composition of weld metal was carried out by the methods of transmission electron diffraction microscopy (TEM) [9, 10].

## Results and Discussion

The welds differ in degree of alloying, namely, total concentration of alloying elements (Si, Mn, Cr, Ni, Cu, Nb, Al) in weld No. 1 amounted to 2.413 wt. %, in weld No. 2 it was - 1.487 wt. %. The main difference in elemental composition of weld metal is observed in concentration of manganese and carbon.

The studies of structure of etched metallographic sections of weld revealed the presence of a large number of second phase particles. As a result of high-speed heating

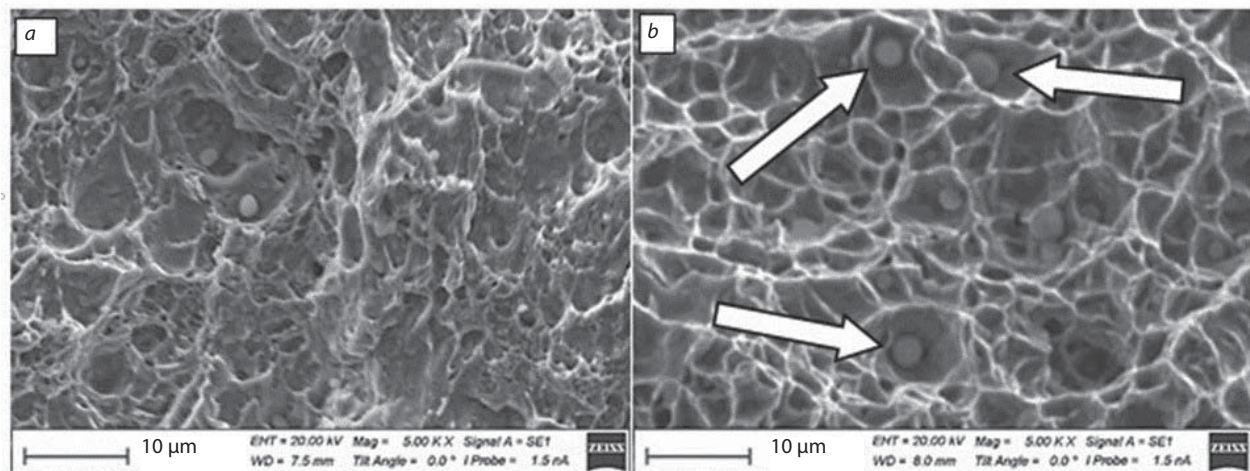


Fig. 1. Viscous fracture facets of metal of welds No. 1 (a) and No. 2 (b). Arrows indicate the second phase particles (b)

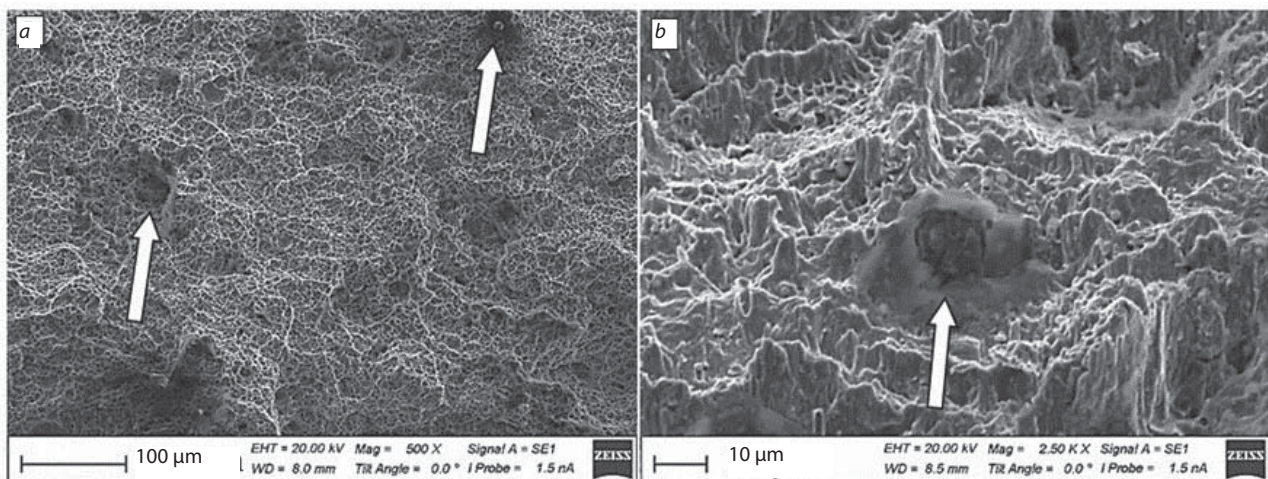


Fig. 2. Viscous fracture surface of metal of weld No. 2. Arrows indicate nonmetallic inclusions

of thin surface layer the etching of steel polished surface by pulsed electron beam results in the formation of microcraters [11] in the region of location of second phase inclusions (carbides, sulfides, oxides, etc.). In weld No. 1 the second phase particles locate chaotically and in weld No. 2 the second phase particles decorate the grain boundaries. The sizes of second phase particles, detected in this way, vary in the limits from 0.8  $\mu\text{m}$  to 5  $\mu\text{m}$  and are identical for both types of welds.

It is established by the method of random intercepts that amount of second phase particles per length unit of secant (linear density of particles) in weld No. 2 is 3.4-fold greater than that in weld No. 1. It is suggested that introduction of carbon-containing addition results in dispersion of inclusions. As a result of it some quantity of inclusions are not detected by SEM method of etched metallographic section, which introduces errors into results.

The studies of fracture surfaces of welds showed that they contained facets of plastic fracture independently of sample number (No.). At the bottom of facets the second phase particles of round shape (Fig. 1, *b*) locate. This is indicative of the fact that the reason of material fracture is the presence of the particles in the given bulk of weld. It should be noted that sizes of plastic fracture facets in weld No. 1 (Fig. 1, *a*) are several times smaller in comparison with weld No. 2 (Fig. 1, *b*). The latter indicates a finer structure being formed in weld with addition.

The fracture of welds contains micropores. The quantity of micropores in fracture of weld No 1 is several times larger as compared to weld No. 2, however, the micropores' sizes in fracture of the weld are 1.8-fold smaller than in weld No. 2. It may be indicative of decrease in diffusion rate of gases when using carbon-containing addition.

The next distinguishing feature of weld fractures is presence of nonmetallic inclusions typical predominantly of weld No. 2 (Fig. 2). As a rule, nonmetallic inclusions are dielectrics; therefore the characteristic feature of electron microscope images of the inclusions is presence of increased level of light spots in material region containing such particles [9, 10]. Sizes of nonmetallic inclusions vary in limits from 10  $\mu\text{m}$  to 15  $\mu\text{m}$ . It should be expected that presence of the inclusions in weld will contribute to its embrittlement.

Thus, analysis of fracture surface structure allows us to speak of the fact that weld No. 2, comprising a comparatively large amount of nonmetallic inclusions, can be more brittle.

By TEM studies it is established that the main phase of welds under study is  $\alpha$ -iron base solid solution. In addition to  $\alpha$ -iron the particles of iron carbide (cementite) and, mostly in weld No. 2, iron silicide of  $\text{Fe}_3\text{Si}$  composition are present.

In bulk of ferrite grains the different types of dislocation substructures are observed. Firstly, in bulk of ferrite grains of both welds a chaotic dislocation substructure with scalar density of  $\sim 3.57 \cdot 10^{10} \text{ cm}^{-2}$  is observed. Secondly, areas with cellular-netlike dislocation substructure are detected.

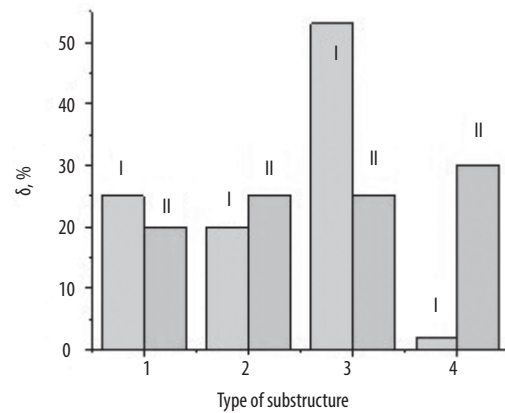


**Fig. 3. Relative content of dislocation substructures revealed in welds under study:**

*1* - ferrite grains with netlike dislocation substructure; *2* - ferrite grains with cellular-netlike dislocation substructure; *3* - ferrite grains with fragmentary dislocation substructure; *4* - ferrite grains of submicron size with chaotically distributed dislocations; I - weld No. 1; II - weld No. 2.

Scalar dislocation density in such a structure amounts to  $2.8 \cdot 10^{10} \text{ cm}^{-2}$  in weld No. 1 and  $3.5 \cdot 10^{10} \text{ cm}^{-2}$  in weld No. 2.

Relative content of dislocation substructures revealed in weld samples under study is presented in Fig. 3. It can be noted that in weld No. 1 a fragmentary (subgranular) substructure is a prevailing type of dislocation substructure. In weld No. 2 the revealed dislocation substructures are present in approximately equal relation and vary in the limits from 20 % to 30 %. Taking into account the fact that fragmentary (subgranular) structure is the substructure preceding a structure with grains of submicron sizes it can be ascertained that in weld No. 2 transformation process in ferrite dislocation substructure proceeded to a greater degree. The latter may be caused by both a higher level of thermomechanical effect on structure of weld No. 2 in welding process and a lower level of alloying of the given steel.

TEM analysis of weld structure enabled us to perform the studies of internal stress fields which manifest themselves as bend extinction contours [10, 12] (Fig. 4). Amplitude of internal stress fields is inversely proportional to transverse size of bend contours, i.e. the smaller the transverse size of contour, the higher the amplitude of material fields. When analyzing electron microscope images of weld structure it was noted that the narrowest contours formed near inclusion/matrix interfaces.

Thus, the inclusions, revealed by the methods of transmission electron microscopy, may be cementite particles, located in bulk and at boundaries of ferrite grains, and particles of iron silicide having round (spherical) shape and located in bulk of ferrite grains. Therefore, second phase inclusions being present in weld are stress concentrators and may be centers of microcrack initiation under mechanical action on material.

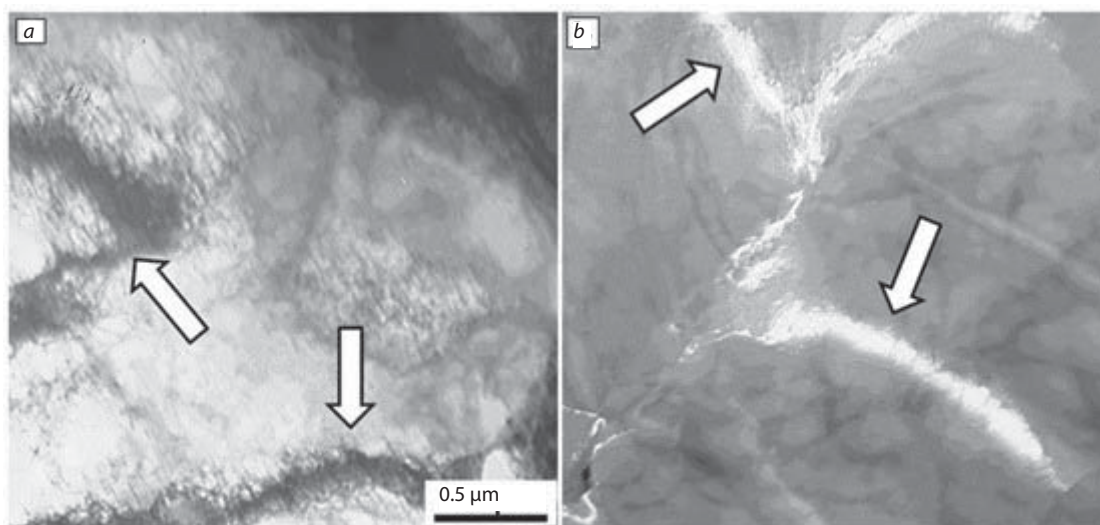


**Fig. 4. TEM images of bend extinction contours in weld structure:**  
*a* - bright field; *b* - dark field in reflection [110]  $\alpha$ -Fe. Arrows indicate contours

Parameters of structure*	Weld No. 1	Weld No. 2
$\langle \rho \rangle$ , $10^{10}$ , $\text{cm}^{-2}$	2.92	3.22
$\rho_{\pm}$ , $10^{10}$ , $\text{cm}^{-2}$	2.04	2.87
$\sigma_f$ , MPa	340	360
$\sigma_d$ , MPa	$285_{\text{plast.}} + 0_{\text{elast.}}$	$335_{\text{plast.}} + 130_{\text{elast.}} = 465$
$\delta$ ( $\text{Fe}_3\text{C}$ )	0.97 % (0.41 % - on boundaries, 0.56 % - inside the grain)	0.30 % (0.20 % - on boundaries, 0.10 % - inside the grain)

\* The designations are the following:  $\langle \rho \rangle$  - scalar dislocation density;  $\rho_{\pm}$  - excess dislocation density;  $\sigma_f$  - contribution to metal strengthening due to retardation of mobile dislocations by 'forest' dislocations;  $\sigma_d$  - contribution to metal strengthening due to internal stress fields (plastic and elastic constituents);  $\delta(\text{Fe}_3\text{C})$  - volume fraction of cementite particles.

On the basis of electron microscope studies of welds the quantitative analysis of steel structure characteristics is presented in the **Table 2**. Scalar ( $\langle \rho \rangle$ ) and excess ( $\rho_{\pm}$ ) dislocation densities as well as volume fraction of cementite ( $\text{Fe}_3\text{C}$ ) were determined; according to the known relationships [12] the estimate of metal strengthening due to presence of dislocation substructure and internal stress fields was done.

It is seen that in metal structure of weld No. 1 the volume fraction of cementite is higher than that in weld No. 2. Scalar and excess dislocation density in metal structure of weld No. 2 is higher than in weld No. 1. Metal strengthening, being introduced by dislocation substructure, was estimated in the research on the basis on known relation [12]:

$$\sigma_d = \sigma_0 + \alpha m G b \sqrt{\langle \rho \rangle}$$

where  $\sigma_0$  is flow stress of nondislocation origin (i.e. caused by other mechanisms of strengthening);  $\alpha$  is parameter characterizing the value of interdislocation interactions;  $m$  is Smidt orientation factor,  $G$  is rigidity modulus of steel;  $b$  – Burgers vector of dislocation. In the Table 2 the value of  $\sigma_0$  was not estimated, therefore the effect of disloca-


tion strengthening was determined only by the  $\langle \rho \rangle$  value. Material strengthening by the particles of second phase was not estimated in the research.

A higher scalar and excess dislocation density in weld No. 2 resulted in a higher value of contribution to metal strengthening caused by retardation of mobile dislocations by 'forest' dislocations ( $\sigma_f$ ) and contribution caused by internal stress fields. The latter indicates a higher level of internal stresses in weld No. 2 and, possibly, a more considerable quantity of stress concentrators which can result in material embrittlement of the given sample.

Commercial tests of welds formed with carbon-containing addition in manufacturing the large-size constructions from low-alloy steel were performed at Novokuznetsk reservoir metalwork plant and validated the increased physical-mechanical characteristics of welds and operational properties of products themselves.

### Conclusion

By the methods of scanning and transmission electron microscopy the studies of structural phase state, defect

substructure and fracture surface of low-alloy steel welds formed with use of carbon-containing addition (weld No. 1) and without (weld No. 2) it have been carried out. The features of distribution of second phase particles are detected, and it is shown that the particles locate chaotically in weld No. 1, and in weld No. 2 they decorate the ferrite grain boundaries. The analysis of fracture surface structure of welds is performed, and presence of nonmetallic inclusions typical mainly of weld No. 2 is revealed, it can indicate its increased brittleness. A quantity of micropores in fracture of weld No. 1 is many times higher than in weld No. 2 which is indicative of decrease in speed of gas diffusion when employing carbon-containing addition. It is shown that structure of weld No. 2 is characterized by higher values of scalar and excess dislocation density, the level of internal stress fields and, possibly, a large quantity of stress concentrators which can result in material embrittlement. The results of study of structure-phase state, defect substructure and fracture surface of welds extend the understanding of role of carbon in increasing the physical-mechanical properties of weld metal and operational properties of weld metalwork as a whole, contribute to development of new carbon-containing welding materials which allow the production of critical large-size constructions from low-alloy steel operating under extreme conditions. 

#### REFERENCES:

- Saini S., Singh K. Recycling of steel slag as a flux for submerged arc welding and its effects on chemistry and performance of welds. *International Journal of Advanced Manufacturing Technology*. 2021. Vol. 114. pp. 1165–1177.
- Makienko V. M., Atnyaev A. V., Belous T. V. Development of Welding Fluxes for Hardfacing Based on Mineral Raw Materials of the Far Eastern Region of Russia. *Inorganic Materials: Applied Research*. 2021. Vol. 12. pp. 558–569.
- Lee J., Lee K., Lee S., Kwon O. M., Kang W.-K., Lim J.-I., Lee H.-K., Kim S.-M., Kwon D. Application of Macro-Instrumented Indentation Test for Superficial Residual Stress and Mechanical Properties Measurement for HY Steel Welded T-Joints. *Materials*. 2021. Vol. 14. pp. 2061 (1-13).
- Bakhmatov P. V., Startsev E. A., Sobolev B. M. Impact and Effect Study of Submerged-Arc Welding Conditions on Structural Changes in Weld Metal. Current Problems and Ways of Industry Development: Equipment and Technologies. *Lecture Notes in Networks and Systems*. 2021. Vol. 200. pp. 65-76.
- Lochan S., Rahul C. Study of weld bead chemical, microhardness & microstructural analysis using submerged arc welding fluxes for linepipe steel applications. *Ceramics International*. 2020. Vol. 45 (15). pp. 24615-24623.
- Kryukov R. E., Kozyreva O. A., Kozyrev N. A. The carbon-fluorine additives for welding fluxes. *Mechanics, Materials Science and Engineering*. 2016. Vol. 2 (2). pp. 5-14.
- Kozyrev N. A., Kryukov R. E., Kryukov N. E., Kovalskiy I. N., Igushev V. F. Technological aspects of using a carbon-fluorine-containing addition in submerged-arc welding. *Welding International*. 2016. Vol. 30 (4). pp. 325-328.
- Koval N. N., Ivanov Yu. F. Evolution of structure of steel surface layer subjected to electron-ion-plasma methods. Tomsk: NTL, 2016. 304 p.
- Egerton F. R. *Physical Principles of Electron Microscopy*. Basel: Springer International Publishing, 2016. 196 p.
- Carter C. B., Williams D. B. *Transmission Electron Microscopy*. Berlin: Springer International Publishing, 2016. 518 p.
- Rotshtein V. P., Proskurovskiy D. I., Ozur G. E., Ivanov Yu. F. Modification of surface layers of metallic materials by low-energy high-current electron beams. Novosibirsk: SB RAS: Nauka, 2019. 348 p.
- Yuriev A. A., Gromov V. E., Ivanov Yu. F., Rubannikova Yu. A., Starostenkov M. D., Tabakov P. Y. Structure and Properties of Lengthy Rails after Extreme Long-Term Operation. *Materials Research Forum LLC*, 2021. 193 p.